Available online at www.sciencedirect.com
SCIENCE DIRECT®
Journal of Organometallic Chemistry 679 (2003) 181–193
Journal of Organometallic Chemistry
www.elsevier.com/locate/jorganchem

Pronounced effects of grinding on rates of intramolecular electron transfer in mixed-valence 1′,2′,1‴,2‴-tetranaphthylmethyl- and 1′,3′,1‴,3‴-tetranaphthylmethyl-biferrocenium triiodides

Teng-Yuan Dong [a,*], Mei-Ching Lin [a], Liangshiu Lee [a,*], Ching-Hung Cheng [a], Shie-Ming Peng [b], Gene-Hsiang Lee [b]

[a] *Department of Chemistry, Center for Nanoscience and Nanotechnology, National Sun Yat-Sen University, Kaohsiung, Taiwan, ROC*
[b] *Department of Chemistry, National Taiwan University, Taipei, Taiwan, ROC*

Received 18 February 2003; received in revised form 4 June 2003; accepted 5 June 2003

Abstract

The X-ray structural determinations of the neutral 1′,2′,1‴,2‴-tetranaphthylmethylbiferrocene and the mixed-valence 1′,3′,1‴,3‴-tetranaphthylmethylbiferrocenium triiodide have been determined. Our Mössbauer measurements for mixed-valence 1′,2′,1‴,2‴-tetranaphthylmethylbiferrocenium triiodide (**1**) and 1′,3′,1‴,3‴-tetranaphthylmethylbiferrocenium triiodide (**2**) indicate that the intramolecular electron-transfer rates in **1** and **2** are quite sensitive to the environmental perturbations caused by the grinding of sample. An interesting finding is that the Mössbauer results indicate that the unground diffusing sample of **1** is valence delocalized on the Mössbauer time scale above 180 K. However, the ground diffusing sample of **1** exhibits a Mössbauer spectrum characteristic of a valence-trapped cation which remains valence-trapped electronic state even at 300 K. The effects of grinding of samples are also observed in the EPR measurements.

Keywords: Mixed-valence 1′,1‴-dinaphthylmethylbiferrocenium; Biferrocenium; Metallocene; Electron transfer

1. Introduction

We undertook the present work in the hope that comparison of molecular structures with the physical properties of 1′,2′,1‴,2‴-tetranaphthylmethylbiferrocenium triiodide **1** and 1′,3′,1‴,3‴-tetranaphthylmethylbiferrocenium triiodide (**2**) would improve our understanding of the factors controlling the rate of intramolecular electron transfer in the solid state for mixed-valence biferroceniun cation. In solution state, the rate of electron transfer for a given mixed-valence biferrocenium cation is influenced by the electronic and vibronic coupling constants between two iron centers and the zero-point energy difference between the two vibronic states. Studies have been concentrated on the extent of electron delocalization and the shape of corresponding intervalence transition (IT) band, and the physical properties have been discussed in light of the Hush model [1] and the PKS model [2]. However, in the case of solid state, it has been recognized that the variations in structural conditions, including lattice dynamics [3–7], cation–cation and cation–anion interactions [8], and the nature of counterion [9–12], can dramatically affect the rate of intramolcular electron transfer. The work to be reported is an extension of our earlier results on the rate of electron transfer in 1′,1‴-dinaphthylmethylbiferrocenium triiodide [13]. To further confirm the correlation of structure and rate of electron transfer, we prepared two new mixed-valence biferrocenium triiodides **1** and **2**.

The series of mixed-valence biferrocenium salts have been studied extensively in the solid state [14]. The first strategy is the use of a series of the mixed-valence biferrocenium with short alkyl substituents (Chart 1, compounds **3a**–**f**) [4–6,15–17]. Compounds **3a**, **3e** and **3f** give valence-localized Mössbauer spectra. At tem-

* Corresponding author. Tel.: +886-7-5253-937; fax: +886-7-5253-908.
E-mail address: dty@mail.nsysu.edu.tw (T.-Y. Dong).

0022-328X/03/$ - see front matter © 2003 Elsevier B.V. All rights reserved.
doi:10.1016/S0022-328X(03)00556-4

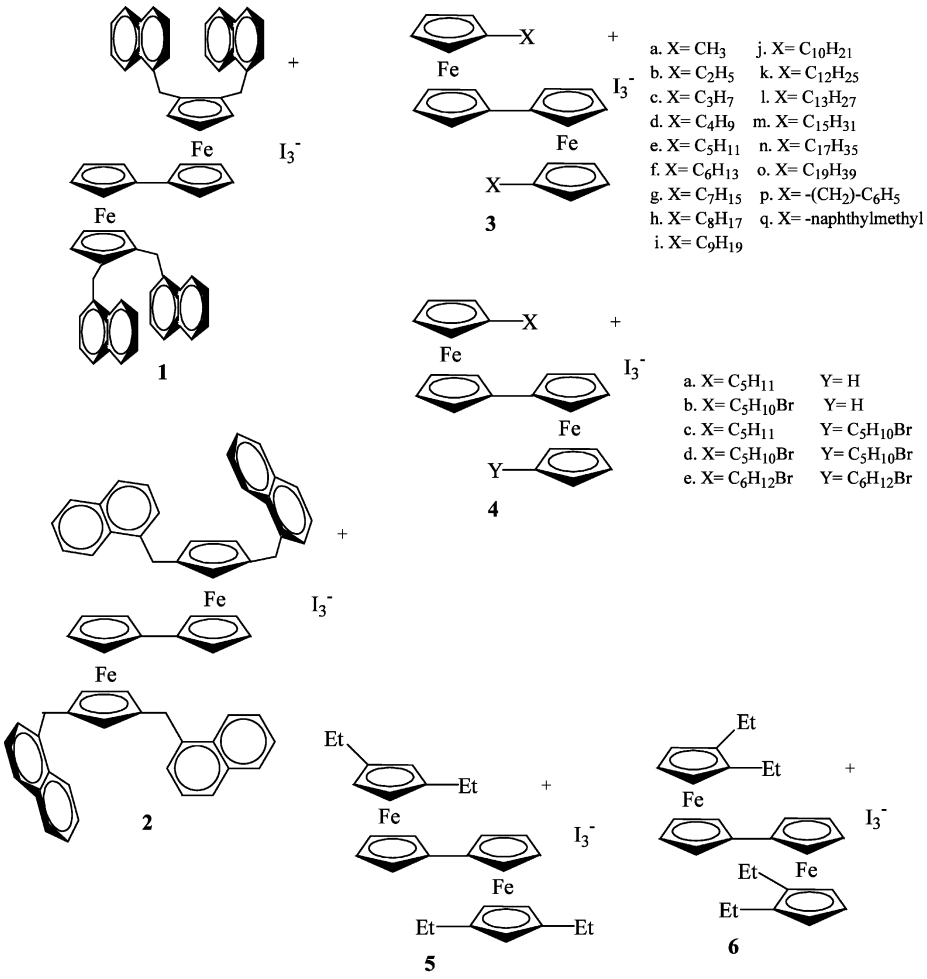

Chart 1.

peratures below 300 K, the spectrum shows two doublets, one for the Fe(II) metallocene and the other for the Fe(III) metallocene (electron-transfer rate $< \sim 10^7$ s^{-1}). However, compounds **3b–d** show temperature-dependent Mössbauer spectra. In each case the two doublets move together with increasing temperature, and eventually become a single 'average-valence' doublet at temperatures of 275, 260 and 275 K, respectively. The second strategy is the use of the mixed-valence biferrocenium salts with long alkyl substituents **3g–o** [18,19]. It has been shown that there is an even–odd character in the number of carbon atoms of the substituents in the relationship between the crystal structure and the mixed-valenced state. The third strategy is the use of the derivatives attached to a planar substituent **3p–q** [13,21]. The 2-phenylethyl and 4-phenylbutyl derivatives of **3p** show the valence detrapping electronic state at temperature of 300 and 160 K, respectively. Recently, we found that the mixed-valence compound **3q** has two distinct crystallographic phases that show the electron-transfer rates are extremely sensitive to changes in the crystal lattice [13]. The crystal in the space group $P\bar{1}$ shows a Mössbauer spectrum characteristic of a valence-detrapped electronic state above 130 K. The crystal in the space group $P2_1/n$ shows a valence-trapped Mössbauer spectrum at 300 K. In **3p** and **3q**, there is a close connection between the mixed-valence state and cation–cation interaction formed through the π–π interaction of the benzene rings.

Very recently, our strategy for systematic design is the use of the derivatives **4a–e** with terminal bromide in the alkyl substituents [14]. The dibromopenthylbiferrocenium triiodide (**4d**) has a detrapped-valence state and the dibromohexylbiferrocenium triiodide has a trapped-valence state. We suggested that the zero-point energy difference plays a crucial role in determining the nature of the intramolecular electron-transfer rate in biferrocenium cation. Finally, to study the influence of the alkyl substituents on the Cp ring, we prepared a series of polyethylbiferrocenium triiodide **5** and **6** [22]. We found that the deviations of the Cp rings from the parallel position correlate quite well with the Mössbauer transition temperature of electronic delocalization-localiza-

tion in mixed-valence biferrocenium cations. We suggested that bending back the Cp rings leads to a larger extent of the metal–ligand interactions.

In this paper, we have prepared two new mixed-valence polynaphthylmethylbiferrocenium triiodide salts to study the influence of naphthylmethyl substituents on the intramolecular electron-transfer rate (Scheme 1). Furthermore, we carried out the X-ray crystal structural determinations, CV measurements, ^{57}Fe Mössbauer analyses, and EPR studies. Here, we report an interesting finding for these particular new mixed-valence compounds that grinding the sample has a pronounced influence on the ^{57}Fe Mössbauer characteristics, EPR measurements and powder X-ray diffraction measurements.

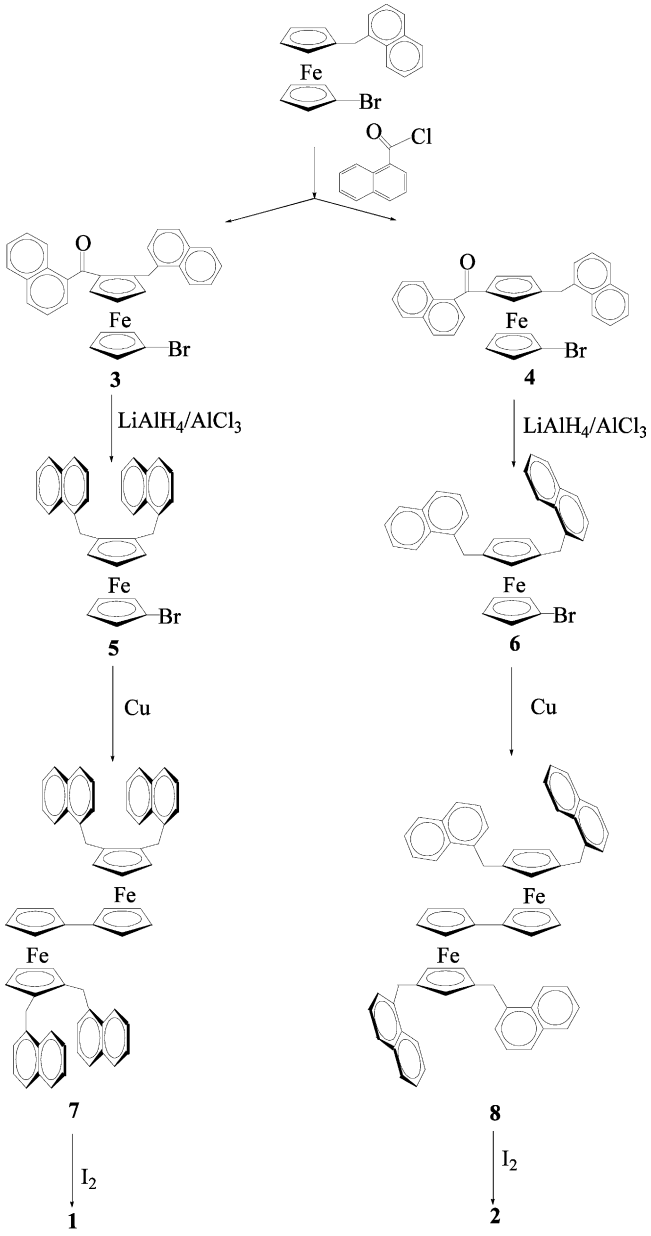

Scheme 1.

2. Results and discussion

Although the physical properties of **1** and **2** are different, it is difficult to assign their structures with certainty solely with NMR spectroscopy. X-ray crystallographic studies of these complexes were undertaken to help us to elucidate the geometric influences on the rate of intramolecular electron transfer. Before the new physical data are described, a summary of single-crystal X-ray structural results obtained for **7** and **2** will be presented.

2.1. Molecular structure of 7

The results of our crystallographic study at room temperature show that **7** crystallizes in the monoclinic space group $P2_1/n$. The structure imposed an inversion center on the biferrocene molecule. The molecule exists in a *trans* conformation with two iron ions on opposite sides of the planar fulvalenide ligand. An ORTEP drawing of the molecule is shown in Fig. 1, and selected bond distances and angles are given in Table 2. As shown in Fig. 1, the naphthylmethyl substituents are at 1′,2′,1‴,2‴-position of Cp rings.

Inspection of the iron to Cp ligand bond lengths (Fe–Cp) shows that the average distance (1.646 Å) is closer to the value of 1.65 Å found [23] for the neutral ferrocene than to the value of 1.70 Å found [24] for

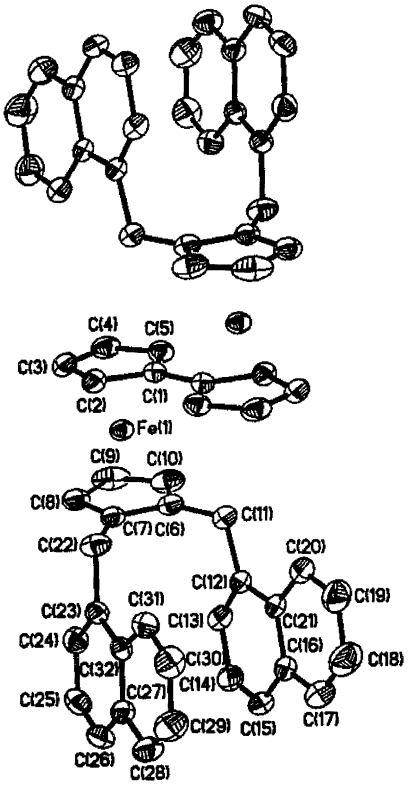

Fig. 1. ORTEP drawing of the neutral biferrocene compound **7**.

Table 1
Experimental and crystal data for the X-ray structures

Compound	**7**	**2**
Formula	$C_{64}H_{50}Fe_2$	$C_{64}H_{50}Fe_2I_3$
Molecular weight	930.74	1311.44
Crystal system	Monoclinic	Monoclinic
Space group	$P2_1/n$	$P2_1/n$
Unit cell dimensions		
a (Å)	8.510(2)	8.8507(6)
b (Å)	8.860(2)	23.848(2)
c (Å)	29.727(4)	12.2528(9)
α (°)	90	90
β (°)	91.42(2)	100.918(2)
γ (°)	90	90
V (Å^3)	2240.6(7)	2539.5(3)
Z	2	2
D_{calc} (g cm^{-3})	1.380	1.715
μ (mm^{-1})	0.692	2.437
λ (Å)	0.71073	0.71073
2θ limits (°)	55	55
Trans coefficient	0.7502–0.8100	0.7456–0.8706
R [a]	0.037	0.0297
R_w [b]	0.1034	0.0647

[a] $R = S(||F_o| - |F_c||)/S|F_o|$.
[b] $R_w = S[(w|F_o| - |F_c|)^2/S(wF_o^2)]^{1/2}$.

Table 2
Selected bond lengths (Å) and bond angles (°) for compounds **7** and **2**

	7	**2**
Bond lengths		
Fe–C(1)	2.053(2)	2.086(3)
Fe–C(2)	2.042(2)	2.063(3)
Fe–C(3)	2.047(3)	2.065(3)
Fe–C(4)	2.034(2)	2.060(3)
Fe–C(5)	2.035(2)	2.061(3)
Fe–C(6)	2.052(2)	2.088(3)
Fe–C(7)	2.052(3)	2.076(3)
Fe–C(8)	2.025(3)	2.081(3)
Fe–C(9)	2.020(3)	2.060(3)
Fe–C(10)	2.035(3)	2.063(3)
C(1)–C(1) [a]	1.465(4)	1.443(5)
C(1)–C(2)	1.422(3)	1.428(4)
C(1)–C(5)	1.427(3)	1.449(4)
C(2)–C(3)	1.419(3)	1.419(4)
C(3)–C(4)	1.401(4)	1.419(4)
C(4)–C(5)	1.414(3)	1.419(4)
C(6)–C(7)	1.417(3)	1.422(4)
C(6)–C(10)	1.416(4)	1.424(4)
C(7)–C(8)	1.422(3)	1.418(4)
C(8)–C(9)	1.425(4)	1.424(4)
C(9)–C(10)	1.398(4)	1.428(4)
I(1)–I(2)		2.9076(3)
Bond angles		
C(2)–C(1)–C(5)	107.3(2)	108(1)
C(1)–C(2)–C(3)	107.7(4)	107(2)
C(2)–C(3)–C(4)	108.8(4)	109(2)
C(3)–C(4)–C(5)	108.4(4)	110(2)
C(1)–C(5)–C(4)	107.8(4)	107(2)
C(7)–C(6)–C(10)	106.1(4)	104(2)
C(6)–C(7)–C(8)	109.4(4)	108(2)
C(7)–C(8)–C(9)	107.4(4)	108(2)
C(8)–C(9)–C(10)	108.4(5)	108(2)
C(6)–C(10)–C(9)	108.7(4)	112(2)
I(2)–I(1)–I(2) [b]		180

[a] Symmetry transformations used to generate equivalent atoms for **7**: $-x+1, -y+1, -z$; for **2**: $-x-1, -y+1, -z$.
[b] Symmetry transformations used to generate equivalent atom: $-x, -y, -z$.

the ferrocenium ion. The average Fe–C bond distance of 2.04 Å is also closer to the value of 2.045 Å found for the neutral ferrocene than to the value of 2.075 Å found for the ferrocenium ion. The dihedral angle between the least-squares planes of the Cp rings, associated with the Fe center is 1.41°, while the two Cp rings are nearly eclipsed with an average staggering angle of 8°.

2.2. Molecular structure of **2**

Compound crystallizes in the monoclinic space group $P2_1/n$ at 150 K. Fig. 2 shows the molecular structure and atomic labeling scheme for the cation and anion. Compound **2** has the usual trans conformation seen in other dialkyl mixed-valence biferrocenium triiodide salts [3–22,25]. Mean bond distance between the iron atom and the five carbon atoms of a given Cp ring is 2.071 Å which lies midway between the 2.045 Å observed for the neutral ferrocene and 2.075 Å observed for the ferrocenium ion [24]. The average Fe–Cp distance (1.678 Å) is also intermediate between the values of 1.65 Å for the neutral ferrocene and 1.70 Å for the ferrocenium ion. The site symmetry imposed on the mixed-valence cation obviously requires that both iron centers of the cation are in equivalent positions at 150 K. This is consistent with our variable-temperature Mössbauer studies for an unground diffusing crystalline sample of **2**. The plane of Cp rings form a dihedral angle of 0.69° with the fulvalenide plane, and the two Cp rings in each ferrocenyl moiety are not perfectly eclipsed but are rotated relative to one another by 11°. From the packing arrangement of **2**, the intermolecular naphthyl–naphthyl (π–π) interaction is not observed between neighbor cations. In $P2_1/n$ phase, the triiodide is strictly linear as required by the inversion symmetry. The I–I bond distance is 2.9076(3) Å, which compares well with other determinations of the symmetric triiodide bond distance.

2.3. Electrochemical results

Electrochemical data for the neutral biferrocenes **7** and **8**, as well as those for some other relevant compounds, are shown in Table 3. The cyclic voltammograms are shown in Fig. 3. These binuclear biferrocenes all show two successive reversible redox waves.

It has been reported that the peak-to-peak ($\Delta E_{1/2}$) separation can gauge the interaction between the two Fe sites in a biferrocenium cation [26]. The separations

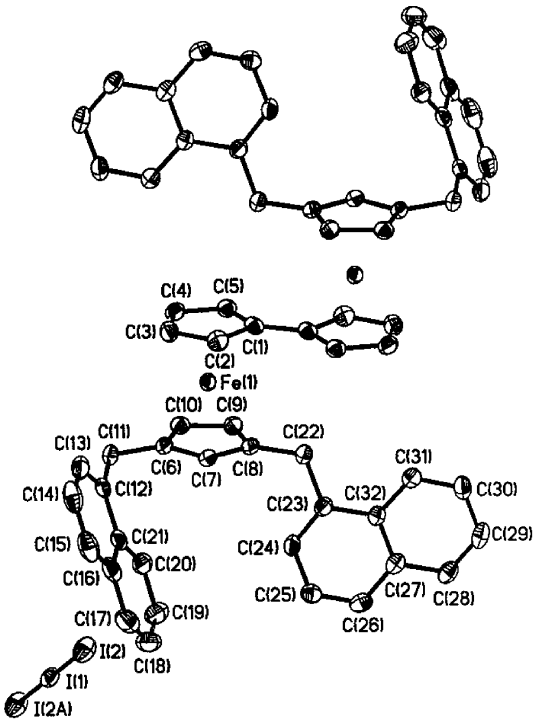

Fig. 2. ORTEP drawing of the cation in the mixed-valence biferrocenium compound **2**.

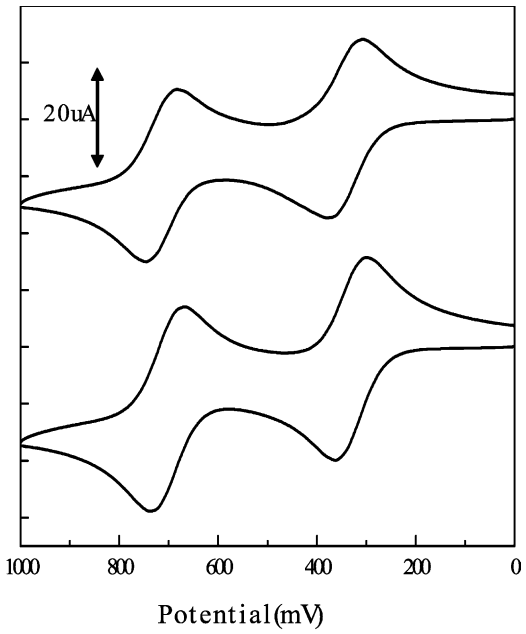

Fig. 3. Cyclic voltammograms of **7** (top) and **8** (bottom), $v = 100$ mV s^{-1}.

between the two redox waves for **7** and **8** are 0.37 and 0.38 V, respectively. In other words, the magnitude of the electronic interaction between the two Fe sites in **7** and **8** is nearly equivalent in solution state. Making a comparison with biferrocene or the corresponding neutral biferrocene **3q**, the electronic interaction between the two Fe centers in **7** and **8** is larger. This is not quite correlative to our solid-state Mössbauer measurements for mixed-valence biferrocenium salts **1** and **2**, which indicate the intramolecular electron-transfer rates of **1** and **2** in solid state are quite sensitive to the environmental perturbations caused by the grinding of sample.

2.4. Fe Mössbauer characteristics

It has been noted that ^{57}Fe Mössbauer spectral properties of 1′,1‴-dialkylbiferrocenium triiodide salts are dependent on sample history [3,4]. To examine this phenomenon more thoroughly, we prepared microcrystalline and diffusing crystalline samples of **1** and **2** as described in Section 4. The variable-temperature ^{57}Fe Mössbauer spectra of an unground microcrystalline sample of **1** are shown in Fig. 4. The various absorption peaks were fitted into Lorentzian lines and the fitting parameters are collected in Table 4. The 80 K Mössbauer spectrum shows two doublets, one with a $\Delta E_Q =$ 0.496 mm s^{-1} (Fe(III) site) and the other with a $\Delta E_Q =$ 1.963 mm s^{-1} (Fe(II) site). Both doublets were fitted to

Table 3
Cyclic voltammetry data for various biferrocenes

Compound	$E_{1/2}$ (V) [a]	$\Delta E_{1/2}$ (V) [b]	ΔE_p (mV) [c]	I_c/I_d [d]	$K_{com}(10^{-5})$ [e]
Ferrocene	0.37		70	1.01	
Biferrocene	0.31	0.31	70	1.01	1.80
	0.62		75	1.01	
3q	0.33	0.35	61		8.6
	0.68		60		
7	0.27	0.37	68	1.09	18.67
	0.64		61	1.15	
8	0.25	0.38	59	1.21	27.57
	0.63		70	1.25	

[a] All half-wave potentials are referred to the Ag/AgCl electrode in the CH_2Cl_2/CH_3CN (1:1) solution.
[b] Peak separation between two waves.
[c] Peak-to-peak separation between the resolved reduction and oxidation wave maxima.
[d] Peak–current ratio between cathode and anode.
[e] K_{com}: comproportionation equilibrium constant.

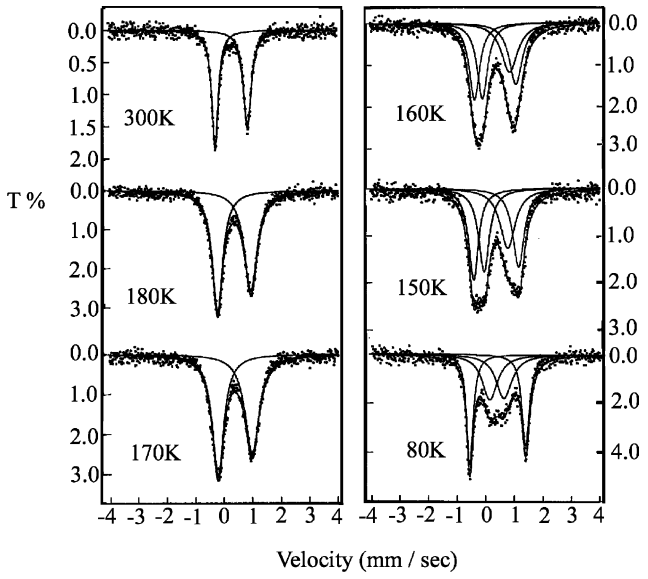

Fig. 4. Variable-temperature ^{57}Fe Mössbauer spectra of an unground microcrystalline sample of **1**.

have the same area. This pattern of two doublets is what is expected for a valence-trapped mixed-valence biferrocenium cation. Increasing the temperature causes the two doublets to move together and eventually to become a valence-detrapped doublet at temperature of 170 K. An interesting finding for this particular new mixed-valence compound is that grinding the sample has a pronounced influence on the rate of electron transfer. The fitting parameters for the variable-temperature Mössbauer spectra for the manually ground microcrystalline sample of **1** are also collected in Table 4. At 80 K, the Mössbauer spectrum shows two doublets ($\Delta E_Q =$ 0.568 and 1.999 mm s^{-1}). At temperatures above 220 K, the spectrum of this sample shows a single doublet which is a characteristic of a valence-detrapped cation in which the electron-transfer rate exceeds $\sim 10^7$s^{-1}. Thus, there is a decrease in the electron-transfer rate as a result of grinding the sample. The dependence of the sample history observed in the series of dialkylbiferrocenium cations has also been seen for **1**. The Mössbauer fitting parameters for the spectra obtained for an unground diffusing crystalline sample of **1** are also collected in Table 4. The Mössbauer results indicate that the unground diffusing crystalline sample is valence delocalized on the Mössbauer time scale in the solid state above 180 K. In comparison with unground microcrystalline sample, there is a 10 K difference in the localized-to-delocalized transition temperature. Actually, this is not a significant difference. However, the ground diffusing crystalline sample of **1** exhibits a Mössbauer spectrum characteristic of a valence-trapped cation (Fe(II), $\Delta E_Q = 1.964$ mm s^{-1}; Fe(III), $\Delta E_Q = 0.501$ mm s^{-1}) which remains valence-trapped electronic state even at 300 K (Fig. 5). Obviously, the intramolecular electron transfer in **1** is quite sensitive to the environmental perturbations caused by the grinding.

Two different preparations of **2** were also examined with variable-temperature Mössbauer spectroscopy. Several unusual observations that have been made for **1** have also been seen for mixed-valence cation **2**. Selected spectra are shown in Figs. 6 and 7, and the fitting parameters are listed in Table 4. In the case of unground microcrystalline sample, the two doublets are seen to move together as the sample temperature is increased, finally becoming a single average doublet at $\sim$120 K. Thus, in comparison with unground microcrystalline sample of **1**, the change of the relative positions on the naphthylmethyl substituents from 1′,2′,1‴,2‴-positions in **1** to 1′,3′,1‴,3‴-position in **2** leads to a reduction by 50 K in the temperature where the mixed-valence cation of **2** transfers an electron faster than the Mössbauer time scale. The effect of grinding sample on the electron-transfer rate observed in **1** has also been observed in the case of microcrystalline sample of **2**. However, it is not a significant difference, only 10 K difference in temperature. For an unground diffusing crystalline sample, the Mössbauer results indicate that the cation is valence delocalized on the time scale above $\sim$140 K. However, it was curious to find that the 300 K Mössbauer spectrum of the ground diffusing crystalline sample consists of valence-trapped and valence detrapped signals. The variable-temperature Mössbauer spectra are shown in Fig. 7. At 80 K, the spectrum shows two doublets, one for Fe(II) metallocene ($\Delta E_Q =$ 2.052 mm s^{-1}) and the other for Fe(III) metallocene ($\Delta E_Q = 0.726$ mm s^{-1}). These two doublets do not coalesce into an 'average-valence' doublet at 300 K as found for the unground sample. The prominent features in the 300 K spectrum are two doublets, one with a $\Delta E_Q = 2.049$ mm s^{-1} and the other with $\Delta E_Q = 0.456$ mm s^{-1}. Both doublets have the same area. Fitting the 300 K spectrum also clearly shows a third doublet with $\Delta E_Q = 1.094$ mm $^{-1}$. This doublet is associated with a valence-detrapped biferrocenium cation. The ratio of valence-localized to valence-delocalized species in the 300 K spectrum is 1.34:1.

Our Mössbauer results indicate that changing the substituent in the biferrocenium cations **1** and **2** leads to dramatic change in the electron-transfer rate in the solid state. We believe that the difference in electron-transfer rate is not due to a difference in the electronic effect of the substituents. The electrochemical measurements for the corresponding neutral biferrocenes **7** and **8** indicated that the electronic coupling between two iron centers in **7** and **8** is nearly equivalent in the solution state. The difference of structural packing arrangements between **1** and **2** undoubtedly alters the potential energy surface of the mixed-valenced molecule.

Table 4
^{57}Fe Mössbauer least-square-fitting parameters

Compound	T (K)	ΔE_Q [a]	δ [b]	Γ [c]	Area ratio (deloc.: loc.)
1 [d]	300	1.133	0.4354	0.336,0.276	
	180	1.176	0.4930	0.538, 0.446	
	170	1.194	0.4984	0.601, 0.495	
	160	1.454	0.4753	0.555, 0.444	
		0.952	0.5115	0.689, 0.448	
	150	1.594	0.4921	0.488, 0.420	
		0.834	0.4871	0.642, 0.461	
	80	1.963	0.5143	0.326, 0.270	
		0.496	0.4837	0.676, 0.655	
1 [e]	300	1.134	0.4386	0.470, 0.436	
	220	1.150	0.4828	0.568, 0.560	
	200	1.443	0.5016	0.691, 0.668	
		1.009	0.4773	0.580, 0.498	
	170	1.676	0.4996	0.614, 0.596	
		0.898	0.4942	0.650, 0.530	
	160	1.719	0.5022	0.585, 0.549	
		0.838	0.5031	0.690, 0.547	
	80	1.999	0.5189	0.328, 0.313	
		0.568	0.5225	0.774, 0.657	
1 [f]	300	1.099	0.4331	0.350, 0.323	
	200	1.137	0.4766	0.506, 0.458	
	180	1.157	0.4992	0.591, 0.564	
	170	1.481	0.4876	0.509, 0.483	
		0.868	0.4884	0.592, 0.483	
	150	1.682	0.4956	0.442, 0.432	
		0.731	0.4949	0.705, 0.529	
	80	1.957	0.5106	0.295, 0.276	
		0.436	0.5065	0.790, 0.672	
1 [g]	300	1.964	0.4283	0.571, 0.585	
		0.501	0.3875	0.522, 0.496	
	80	2.081	0.5118	0.313, 0.282	
		0.550	0.4933	0.796, 0.785	
2 [d]	300	1.106	0.4328	0.359, 0.346	
	140	1.171	0.5181	0.537, 0.418	
	130	1.190	0.5286	0.568, 0.460	
	120	1.209	0.5337	0.648, 0.472	
	110	1.284	0.6213	0.518, 0.478	
		1.170	0.4538	0.605, 0.501	
	80	1.431	0.5756	0.626, 0.543	
		1.060	0.5019	0.795, 0.534	
2 [e]	300	1.091	0.4298	0.340, 0.329	
	150	1.167	0.5096	0.597, 0.524	
	130	1.211	0.5250	0.687, 0.573	
	120	1.549	0.5263	0.786, 0.715	
		1.059	0.4987	0.646, 0.400	
	110	1.550	0.5270	0.741, 0.682	
		1.053	0.5062	0.744, 0.436	
	80	1.624	0.5344	0.709, 0.585	
		0.974	0.4762	0.810, 0.478	
2 [f]	300	1.089	0.4313	0.282, 0.271	
	140	1.140	0.5115	0.441, 0.361	
	120	1.279	0.5280	0.484, 0.319	
		1.005	0.5170	0.559, 0.351	
	110	1.277	0.5282	0.512, 0.348	
		1.018	0.5163	0.675, 0.384	
	100	1.299	0.5298	0.507, 0.360	
		1.009	0.5082	0.774, 0.408	
	80	1.344	0.5389	0.516, 0.387	
		0.990	0.5051	0.789, 0.403	
2 [g]	300	2.049	0.4288	0.326, 0.309	1:1.3
		1.094	0.4346	0.419, 0.454	
		0.456	0.4402	0.349, 0.342	

Table 4 (*Continued*)

Compound	T (K)	ΔE_Q [a]	δ [b]	Γ [c]	Area ratio (deloc.: loc.)
	150	2.077	0.4913	0.290, 0.291	1:2.3
		1.243	0.5159	0.582, 0.506	
		0.580	0.4954	0.602, 0.539	
	120	2.080	0.5089	0.303, 0.302	1:3.3
		1.335	0.5691	0.534, 0.548	
		0.655	0.5173	0.663, 0.668	
	110	2.082	0.5109	0.319, 0.316	1:3.6
		1.428	0.5406	0.589, 0.514	
		0.636	0.4896	0.650, 0.582	
	100	2.086	0.5129	0.300, 0.311	1:4.4
		1.417	0.5252	0.482, 0.480	
		0.609	0.4902	0.719, 0.610	
	80	2.052	0.5169	0.374, 0.371	
		0.726	0.4986	0.722, 0.643	

[a] Quadrupole-splitting in mm s^{-1}.
[b] Isomer shift referred to iron foil in mm s^{-1}.
[c] Full width (in mm s^{-1}) at half-height taken from the least-squares-fitting program. The width for the line at more positive velocity is listed first for each doublet.
[d] Unground microcrystalline sample.
[e] Ground microcrystalline sample.
[f] Unground diffusing crystalline sample.
[g] Ground diffusing crystalline sample.

The influence of grinding sample on physical properties has been well studied for spin crossover transitions [27]. In the case of mixed-valenced biferrocenium salts, Hendrickson found a reduction of the electron-transfer rate in mixed-valence 1′,1‴-dibenzylbiferrocenium triiodide (**3p**, $n = 1$) as a result of mechanical grinding [21]. A change in valence for a transition-metal complex is generally accompanied by the coordination sphere reorganization. When an intramolecular electron transfer occurs in a biferrocenium cation, the two Cp rings bound to the Fe(II) ion move away from the metal to adjust their distance to the larger dimension appropriate for a $(Cp)_2Fe^{III}$ moiety. At the same time, the dimensions of the $(Cp)_2Fe^{III}$ moiety contract to those of a $(Cp)_2Fe^{II}$ moiety. Hendrickson suggested that what is affecting the Mössbauer spectrum and imparting the temperature dependence is the onset of lattice dynamics (a second-order phase transition) [15]. As the temperature of a compound is increased, the thermal energy could achieve the value necessary to trigger on a cooperative change in the crystal lattice. Hendrickson suggested that the grinding would introduce a higher concentration of defects which create kinetic barriers to domain growth so that metastable domains posses

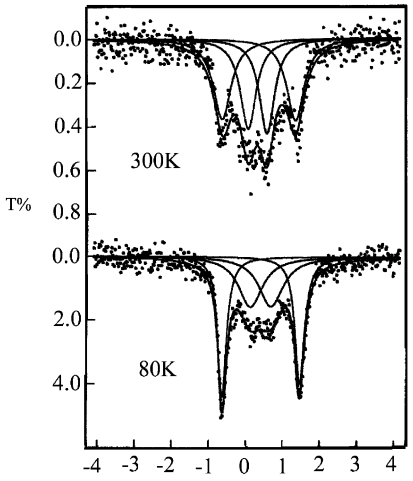

Fig. 5. Variable-temperature ^{57}Fe Mössbauer spectra of a ground diffusing crystalline sample of **1**.

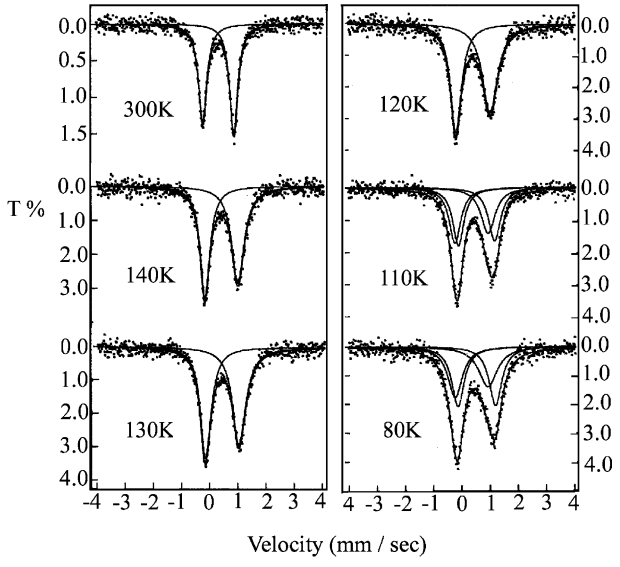

Fig. 6. Variable-temperature ^{57}Fe Mössbauer spectra of an unground microcrystalline sample of **2**.

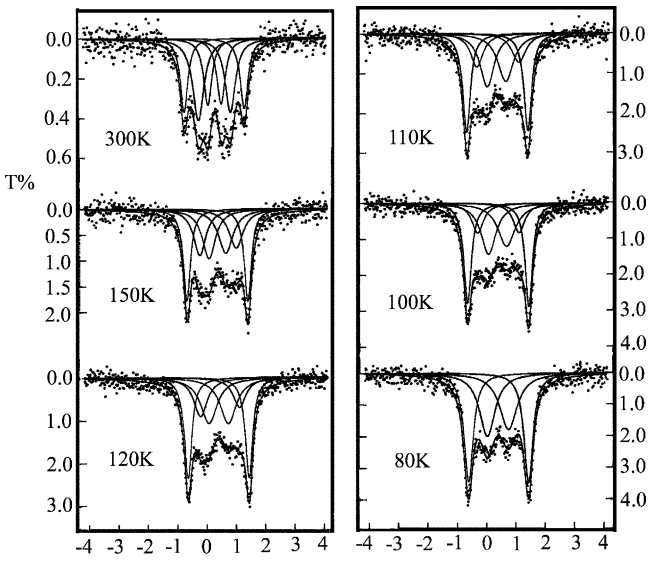

Fig. 7. Variable-temperature ^{57}Fe Mössbauer spectra of a ground diffusing crystalline sample of **2**.

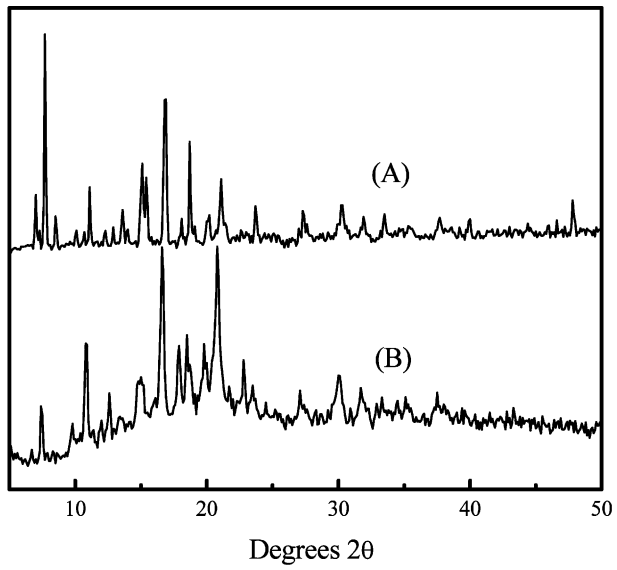

Fig. 8. XRD patterns of unground diffusing crystalline sample of **2** (A) and ground diffusing crystalline sample of **2** (B).

insufficient time and thermal energy to effect a complete conversion. Additionally, defects certainly weaken the cooperative interaction between molecules. In our cases, we would like to suggest that grinding causes a change in structure. This conclusion can be made from the studies of powder X-ray diffraction and EPR discussed in the following section.

2.5. Powder X-ray diffraction

To understand the origin of the effects of grinding on the Mössbauer behavior of samples **1** and **2**, powder X-ray diffraction (XRD) patterns were carried out at 300 K. Grinding samples of diffusing crystalline compounds of **1** and **2** does indeed alter the spectroscopic properties. The XRD patterns of unground and ground diffusing crystalline samples of **2** are shown in Fig. 8, and the XRD patterns of unground and ground diffusing crystalline samples of **1** are available in the supplementary material. A comparison of the pattern for the unground diffusing crystalline sample with that obtained for the ground diffusing crystalline sample seems to indicate that there is a change in structure upon grinding. As can be seen, there are changes in peak positions and intensities with grinding. This observation is also consistent with our EPR studies.

2.6. Electron paramagnetic resonance

For a mononuclear ferrocenium cation with no low-symmetry crystal field distortion, an axial-type spectrum will be observed with $g_{||} = 6$ and $g_{\perp} = 0$ [28]. As the low-symmetry crystal field increase, both $g_{||}$ and $g_{\perp}$ approach a value of 2. In the case of a binuclear mixed-valence biferrocenium cation, the value of g tensor anisotropy ($\Delta g = g_{||} - g_{\perp}$) can be used as a rough estimate of the nature of the electronic ground state of the cation. Here, we are interested in studying the influence of grinding on the electronic ground state by EPR technique [21].

X-band EPR spectra were run for the sample of **1** and **2** at 77 K, and the g values evaluated from these spectra and other related EPR spectra are collected in Table 5. The 77 K spectra of unground microcrystalline and crystalline samples of **1** are clearly typical axial-type spectra ($g_{||} \approx 3.5$ and $g_{\perp} \approx 1.8$) as found for the most 1′,1‴-dialkylbiferrocenium cations [14,21]. The Δg values indicate that the samples exhibits a localized EPR spectra (electron-transfer rate $<$ EPR time scale $\sim 10^{10}$ s^{-1}), and this observation is consistent with our Mössbauer studies. Surprisingly, the 77 K spectra of

Table 5
EPR data

Compound [a]	$g_{||}$	$g_{\perp}$
3q ($P\bar{1}$ phase) [b]	3.16	1.91
3q ($P2_1$/n phase) [b]	3.67, 2.85	2.01, 1.79
1 [c]	3.54	1.79
1 [d]	3.64	1.91, 1.63
1 [e]	3.57	1.76
1 [f]	3.59, 3.25	1.92, 1.64
2 [c]	3.39	1.85
2 [d]	3.29	1.88
2 [e]	3.18	1.91
2 [f]	3.18	1.90

[a] Powder sample.
[b] From Ref. [15].
[c] Unground microcrystalline sample.
[d] Ground microcrystalline sample.
[e] Unground diffusing crystalline sample.
[f] Ground diffusing crystalline sample.

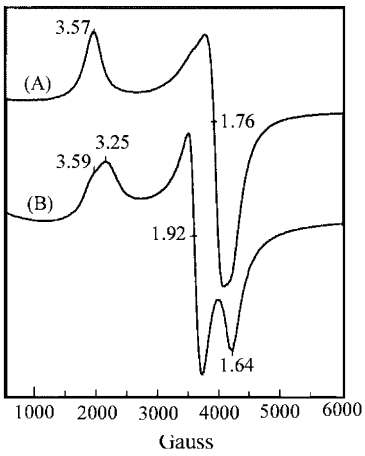

Fig. 9. EPR spectra of unground diffusing crystalline sample of **1** (A) and ground diffusing crystalline sample of **1** (B).

ground microcrystalline and crystalline samples consist of two $g_{||}$ signals and two $g_{\perp}$ signals. As shown in Fig. 9, the EPR spectrum of ground diffusing crystalline sample of **1** shows two $g_{||}$ signals at 3.59 (shoulder) and 3.25 and two $g_{\perp}$ signals at 1.92 and 1.64. Obviously, this is an overlapping of two sets of valence-trapped EPR signals. We believe that the grinding causes a change in structure. The cation with different structure would exhibit different EPR signals.

In the case of mixed-valence cations **2**, the EPR spectra are not quite sensitive to the grinding. All of the microcrystalline samples and crystalline samples (unground and ground) show typical axial-type EPR signals ($g_{||} \approx 3.2$ and $g_{\perp} \approx 1.9$).

3. Conclusion

In this paper, we demonstrate that the minor perturbations caused the substituents on the Cp ring have pronounced influence on the electronic structure of mixed-valence biferrocenium cation. Our Mössbauer, XRD and EPR results indicated that the structural changes created by manual grinding play an important role in intramolecular electron transfer. The grinding effects have been well studied for spin crossover compounds [27]. Here, we provide two new mixed-valence biferrocenium triiodide salts in which the intramolecular electron-transfer rate can be easy to switch on and off on the Mössbauer time scale by a simple process of grinding.

4. Experimental

4.1. General information

All manipulations involving air-sensitive materials were carried out by using standard Schlenk techniques under an atmosphere of N_2. Chromatography was performed on silica gel. Dichloromethane was dried over CaH_2. The sample of 1-naphthylmethyl-1′-bromoferrocene was prepared according to our earlier reported procedure [13].

4.2. Acylation of 1-naphthylmethyl-1′-bromoferrocene

The acylating reagent was made-up according to the Friedel–Crafts synthesis by mixing 2.2 ml (14.8 mmol) of 1-naphthly chloride and excess of $AlCl_3$ in dried CH_2Cl_2 (50 ml) at 0 °C under N_2. The excess of $AlCl_3$ was filtered off with glass wool.

The acylating reagent was added by means of a dropping funnel over a period of 1 h to a solution of 1-naphthylmethyl-1′-bromoferrocene (6 g) in dried CH_2Cl_2 (100 ml) at 0 °C. The reaction mixture was stirred for 6 h and then poured into an ice-water mixture. The resulting mixture was separated after the reduction of ferrocenium cation with aqueous $Na_2S_2O_3$. The organic layer was washed with saturated aqueous $NaHCO_3$ and with H_2O, and then it was dried over $MgSO_4$. The solvent was removed under reduced pressure.

The red oily residue was chromatographed. The first band eluted with hexane/EA (97.5/2.5) was the starting material. The second band was compound **3** (red solid, 1.67 g, 20% yield). The third band eluted with hexane/EA (95/5) was compound **4** (red solid, 2.49 g, 30% yield). The physical properties of **3** are as follows. ^{1}H-NMR ($CDCl_3$, ppm): δ 4.17 (d, 2H, Cp), 4.34 (d, 2H, Cp), 4.41 (s, 2H, Cp), 4.46 (d, 1H, Cp), 4.82 (dd, 2H, $-CH_2-$), 7.43 ~ 7.54 (m, 7H, –naphthyl), 7.73 (dd, 2H, –naphthyl), 7.87 ~ 7.94 (m, 3H, –naphthyl), 8.21 (dd, 2H, –naphthyl). Mass spectrum: $[M]^+$ at m/z 558, 560. M.p.: 154–155 °C. Anal. Calc. for $C_{32}H_{23}BrFeO$: C, 68.72; H, 4.15. Found: C, 68.83; H, 4.21%. The properties of **4** are as follows. ^{1}H-NMR ($CDCl_3$, ppm): δ 4.16 (dd, 2H, Cp), 4.20 (s, 2H, $-CH_2-$), 4.26 (s, 1H, Cp), 4.50 (dd, 2H, Cp), 4.73 (d, 1H, Cp), 4.86 (d, 1H, Cp), 7.33 (t, 1H, –naphthyl), 7.41 ~ 7.54 (m, 6H, –naphthyl), 7.74 (dd, 2H, –naphthyl), 7.89 (m, 2H, –naphthyl), 7.96 (t, 1H, –naphthyl), 8.10 (t, 1H, –naphthyl), 8.26 (dd, 1H, –naphthyl). Mass spectrum: $[M]^+$ at m/z 558, 560. Anal. Calc. for $C_{32}H_{23}BrFeO$: C, 68.72; H, 4.15. Found: C, 68.98; H, 4.12%.

4.3. Reduction of 3 and 4

The reduction reaction was carried out by carefully adding, with stirring, small portions of $AlCl_3$ to a mixture of the corresponding ferrocene compound and $LiAlH_4$ in dry ether. After 2 h, the excess of H_2O was added to the yellow solution, and the ether layer was separated. The ether layer was washed with H_2O and dried over $MgSO_4$. After evaporation of the solvent, the

crude product was chromatographed, eluting with hexane/EA (95/5). The first band was the desired compound (~95% yield). The physical properties of **5** are as follows. ^{1}H-NMR ($CDCl_3$, ppm): δ 4.10 (s, 5H, Cp), 4.33 (s, 4H, –CH_2–), 4.41 (t, 2H, Cp), 7.20 (d, 2H, –naphthyl), 7.32 (t, 2H, –naphthyl), 7.54 (dd, 4H, –naphthyl), 7.73 (d, 2H, –naphthyl), 7.89 (dd, 2H, –naphthyl), 8.11 (dd, 2H, –naphthyl). Mass spectrum: $[M]^+$ at *m*/*z* 544, 546. M.p.: 143–144 °C. Anal. Calc. for $C_{32}H_{25}BrFe$: C, 70.48; H, 4.62. Found: C, 69.65; H, 4.62%. The physical properties of **6** are as follows. ^{1}H-NMR ($CDCl_3$, ppm): δ 4.04 (t, 2H, Cp), 4.11 (d, 2H, Cp), 4.14 (s, 1H, Cp), 4.18 (s, 4H, –CH_2–), 4.37 (t, 2H, Cp), 7.31 (d, 2H, –naphthyl), 7.42 (t, 2H, –naphthyl), 7.52 (m, 4H, –naphthyl), 7.76 (d, 2H, –naphthyl), 7.87 (dd, 2H, –naphthyl), 8.11 (dd, 2H, –naphthyl). Mass spectrum: $[M]^+$ at *m*/*z* 544, 546. M.p.: 127–128 °C. Anal. Calc. for $C_{32}H_{25}BrFe$: C, 70.48; H, 4.62. Found: C, 70.05; H, 4.62%.

4.4. Ullmann coupling reaction of 5 and 6

A mixture of the corresponding bromoferrocene (**5** or **6**, 1 g) and activated Cu (5 g) was heated under N_2 at 110–120°C for 24 h. After cooling to room temperature (r.t.), the reaction mixture was repeatedly extracted with CH_2Cl_2 until the CH_2Cl_2 extracts appeared colorless. The extracts were evaporated and chromatographed. The first band eluted with hexane/EA (98/2) yields the starting material. Continued elution with EA afforded the desired compound. Compounds **7** (20% yield) and **8** (33% yield) were recrystallized from benzene + hexane. ^{1}H-NMR of **7** ($CDCl_3$, ppm): δ 3.93 (d, 8H, –CH_2–), 4.01 (d, 6H, Cp), 4.40 (d, 8H, Cp), 6.98 (d, 4H, –naphthyl), 7.18 (t, 4H, –naphthyl), 7.45 (m, 8H, –naphthyl), 7.60 (d, 4H, –naphthyl), 7.79 (dd, 4H, –naphthyl), 7.94 (dd, 4H, –naphthyl). Mass spectrum: $[M]^+$ at *m*/*z* 930. M.p.: 232–233 °C. Anal. Calc. for $C_{64}H_{50}Fe_2$: C, 82.59; H, 5.41. Found: C, 82.43; H, 5.45%. ^{1}H-NMR of **8** ($CDCl_3$, ppm): δ 3.85 (s, 8H, –CH_2–), 3.96 (s, 4H, Cp), 4.03 (s, 2H, Cp), 4.25 (s, 4H, Cp), 4.37 (s, 4H, Cp), 7.14 (d, 4H, –naphthyl), 7.34 (t, 4H, –naphthyl), 7.47 (m, 8H, –naphthyl), 7.68 (d, 4H, –naphthyl), 7.83 (dd, 4H, –naphthyl), 7.97 (dd, 4H, –naphthyl). Mass spectrum: $[M]^+$ at *m*/*z* 930. M.p.: 215–216 °C. Anal. Calc. for $C_{64}H_{50}Fe_2$: C, 82.59; H, 5.41. Found: C, 82.19; H, 5.41%.

4.5. Mixed-valence compounds 1 and 2

Samples of these mixed-valence compounds were prepared by adding a benzene solution containing a stoichiometric amount of iodine to a benzene solution of the corresponding biferrocene at 0 °C. The resulting dark green crystals were filtered and washed repeatedly with cold hexane. A microcrystalline sample was prepared by rapidly adding hexane into a CH_2Cl_2 solution containing the corresponding biferrocenium triiodide. A diffusing crystalline sample was prepared by slowly diffusing a layer of hexane into a layer of CH_2Cl_2 solution containing the corresponding biferrocenium triiodide salt in a test tube. Elemental analyses of the two different preparations were identical within experimental error. Anal. Calc. for **1** ($C_{64}H_{50}Fe_2I_{3.5}$): C, 55.91; H, 3.67. Found: C, 55.23; H, 3.86%. Anal. Calc. for **2** ($C_{64}H_{50}Fe_2I_3$): C, 58.61; H, 3.84. Found: C, 58.60; H, 3.87%.

4.6. Physical methods

^{57}Fe Mössbauer measurements were made on a constant-velocity instrument which has been previously described [25]. The absolute temperature accuracy is estimated to be $\pm$1 K, while the relative precision is $\pm$ 0.5 K. Computer fitting of the ^{57}Fe Mössbauer data to Lorentzian lines were carried out with a modified version of a program previously reported [29]. Velocity calibrations were made using a 99.99% pure iron foil. Typical line widths for all three pairs of iron lines fell in the range 0.24–0.27 mm s^{-1}. Isomer shifts are reported relative to the iron foil at 300 K. It should be noted that the isomer shifts illustrated in the figures are plotted as experimentally obtained. Tabulated data is provided.

^{1}H-NMR spectra were run on a Varian INOVA-500MHz FT-NMR spectrometer. Mass spectra were obtained with a VG-BLOTECH-QUATTRO 5022 system. X-ray powder diffraction patterns were obtained on a Bruker D8 Advance powder diffractometer equipped with a copper X-ray tube with scan step of 0.1° s^{-1}. Electron paramagnetic resonance data (X-band) were collected with a Bruker EMX-10 spectrometer. The magnetic field was calibrated with a Bruku ER 035M NMR gaussmeter. DPPH was used to gauge the microwave frequency. A direct-immersion dewar, which was inserted into the cavity, was used to obtain 77 K data.

Electrochemical measurements were carried out with a BAS 100W system. CV was performed with a stationary glassy carbon working electrode, which was cleaned after each run. These experiments were carried out with 1×10^{-3} M solution of biferrocene in dry CH_2Cl_2/CH_3CN (1:1) containing 0.1 M of (n-$C_4H_9)_4NPF_6$ as supporting electrolyte. The potentials quoted in this work are relative to a Ag/AgCl electrode at 25 °C. Under these conditions, ferrocene shows a reversible one-electron oxidation wave ($E_{1/2} = 0.37$ V).

4.7. Structural determination of 7

An orange crystal ($0.50 \times 0.40 \times 0.25$ mm^3), which was grown when a layer of hexane was allowed to slowly diffuse into a CH_2Cl_2 solution of **7**, was used for data

collection at 298 K. Cell dimensions (obtained from 25 reflections) and space group data were obtained by standard methods on Siemens SMART CCD XRD. The $\theta-2\theta$ scan technique was used to record the intensities for all reflections for which $2\theta < 55^\circ$. Absorption corrections were made with empirical ψ rotation. Of the 5134 reflections collected, there were 5134 reflections with $F_o^2 > 2\sigma(F_o)^2$, where $\sigma(F_o)^2$ values were estimated from counting statistics. These data were used in the final refinement of the structural parameters. The X-ray crystal data are summarized in Table 1. A direct method was used to determine the heavy-atom positions, which phased the data sufficiently well to permit location of the remaining non-hydrogen atoms from Fourier synthesis. All non-hydrogen atoms were refined anisotropically. During the final cycles of refinement, fixed hydrogen contributions with C–H bond lengths fixed at 0.95 Å were applied. The selected bond distances and angles are given in Table 2. Listings of the final positional parameters for all atoms and thermal parameters are given as supplementary material.

4.8. Structural determination of 2

A dark black crystal ($0.50 \times 0.40 \times 0.25$ mm^3) was obtained by following the same procedure as described for **7**. Data were collected to a 2θ value of 55° on Nonious CAD4 Kappa Axis XRD at 150 K. Absorption corrections were also made. The unit cell dimensions were obtained from 25 reflections. Of the 21555 reflections collected, there were 5834 with $F_o^2 > 2\sigma(F_o)^2$. These data were used in the final refinement. Structure refinement was carried out in the same manner as described for **7**. Details of data collection and cell parameters are given in Table 1. The selected bond distances and angles are given in Table 2. Listings of the final positional parameters for all atoms and thermal parameters are given as supplementary material.

5. Supplementary material

The variable-temperature Mössbauer spectra of ground microcrystalline sample of **1**, unground diffusing crystalline sample of **1**, ground microcrystalline sample of **2**, and unground diffusing crystalline sample of **2** are available from the author on request. The XRD patterns of unground and ground diffusing crystalline samples of **1** are also available. Tables listing the final positional parameters for all atoms, the complete tables of bond distances and angles, and thermal parameters are also available. Crystallographic data for the structural analysis have been deposited with the Cambridge Crystallographic Data Centre, CCDC nos. 198506 and 198507 for compounds **7** and **2**, respectively. Copies of this information may be obtained free of charge from The Director, CCDC, 12 Union Road, Cambridge CB2 1EZ, UK (Fax: +44-1223-336033; e-mail: deposit@ccdc.cam.ac.uk or www: http://www.ccdc.cam.ac.uk).

Acknowledgements

Acknowledgements are made to the National Science Council (Taiwan), the Department of Chemistry, and Center for Nanoscience and Nanotechnology at National Sun Yat-Sen University for financial support.

References

[1] N.S. Hush, Prog. Inorg. Chem. 8 (1967) 391.
[2] K.Y. Wong, P.N. Schatz, Prog. Inorg. Chem. 28 (1981) 369.
[3] M.J. Cohn, T.-Y. Dong, D.N. Hendrickson, S.J. Geib, A.L. Rheingold, J. Chem. Soc. Chem. Commun. (1985) 1095.
[4] T.-Y. Dong, D.N. Hendrickson, K. Iwai, M.J. Cohn, A.L. Rheingold, H. Sano, S. Motoyama, J. Am. Chem. Soc. 107 (1985) 7996.
[5] S. Iijima, R. Saida, I. Motoyama, H. Sano, Bull. Chem. Soc. Jpn. 54 (1981) 1375.
[6] S. Nakashima, Y. Masuda, I. Motoyama, H. Sano, Bull. Chem. Soc. Jpn. 60 (1987) 1673.
[7] M. Kai, M. Katada, H. Sano, Chem. Lett. (1988) 1523.
[8] T. Kambara, D.N. Hendrickson, T.-Y. Dong, M.J. Cohn, J. Chem. Phys. 86 (1987) 2362.
[9] T.-Y. Dong, T. Kambara, D.N. Hendrickson, J. Am. Chem. Soc. 108 (1986) 5857.
[10] T.-Y. Dong, C.C. Schei, T.L. Hsu, S.L. Lee, S. Li, Inorg. Chem. 30 (1991) 2457.
[11] R.J. Webb, S.J. Geib, D.L. Staley, A.L. Rheingold, D.N. Hendrickson, J. Am. Chem. Soc. 112 (1990) 5031.
[12] R.J. Webb, A.L. Rheingold, S.J. Geib, D.L. Staley, D.N. Hendrickson, Angew. Chem. Int. Ed. Engl. 28 (1989) 1388.
[13] T.-Y. Dong, P.H. Ho, X.Q. Lai, Z.W. Lin, K.J. Lin, Organometallics 19 (2000) 1096.
[14] T.-Y. Dong, L.S. Chang, G.H. Lee, S.M. Peng, Organometallics 21 (2002) 4192.
[15] D.N. Hendrickson, S.M. Oh, T.-Y. Dong, T. Kambara, M.J. Cohn, M.F. Moore, Comments Inorg. Chem. 4 (1985) 329.
[16] T.-Y. Dong, D.N. Hendrickson, C.G. Pierpont, M.F. Moore, J. Am. Chem. Soc. 108 (1986) 963.
[17] (a) S. Nakashima, M. Katada, I. Motoyama, H. Sano, Bull. Chem. Soc. Jpn. 60 (1987) 2253;
(b) S. Nakashima, M. Katada, I. Motoyama, H. Sano, Bull. Chem. Soc. Jpn. 59 (1986) 2923;
(c) S. Nakashima, T. Oka, T. Okuda, M. Watanabe, Inorg. Chem. 38 (1999) 4005.
[18] S. Nakashima, S. Nakszaki, H. Sakai, M. Watanabe, I. Motoyama, M. Sato, Inorg. Chem. 37 (1998) 1959.
[19] S. Nakashima, Y. Ueki, H. Sakai, J. Chem. Soc. Dalton Trans. (1995) 513.
[20] (a) T.-Y. Dong, X.Q. Lai, Z.W. Lin, K.J. Lin, Angew. Chem. Int. Ed. Engl. 36 (1997) 2002;
(b) S. Nakashima, A. Hori, H. Sakai, M. Watanabe, I. Motoyama, J. Organomat. Chem. 542 (1997) 271.
[21] R.J. Webb, T.-Y. Dong, C.G. Pierpont, S.R. Boone, R.K. Chadha, D.N. Hendrickson, J. Am. Chem. Soc. 113 (1991) 4806.
[22] T.-Y. Dong, S.H. Lee, C.K. Chang, H.M. Lin, K.J. Lin, Organometallics 16 (1997) 2773.
[23] P. Seiler, J.D. Dunitz, Acta Crystallogr. Sect. B 35 (1979) 1068.

[24] N.J. Mammano, A. Zalkin, A. Landers, A.L. Rheingold, Inorg. Chem. 16 (1977) 297.
[25] T.-Y. Dong, C.C. Schei, M.Y. Hwang, T.Y. Lee, S.K. Yeh, Y.S. Wen, Organometallics 11 (1992) 573.
[26] (a) H. Atzkern, B. Huber, F.H. Köhler, G. Müller, R. Müller, Organometallics 10 (1991) 238;
(b) E.E. Bunel, P. Campos, P. Ruz, L. Valle, I. Chadwick, M.S. Ana, G. Gonzalez, J.M. Manriquez, Organometallics 7 (1988) 474;
(c) D.O. Cowan, P. Shu, F.L. Hedberg, M. Rossi, T.J. Kistenmacher, J. Am. Chem. Soc. 101 (1979) 1304;
(d) R. Moulton, T.W. Weidman, K.P.C. Vollhardt, A.J. Bard, Inorg. Chem. 25 (1986) 1846;
(e) D. Obendorf, H. Schottenberger, C. Rieker, Organometallics 10 (1991) 1293.
[27] G. Ritter, E. Kong, W. Irler, H.A. Goodwin, Inorg. Chem. 17 (1978) 224.
[28] (a) R. Prins, A. Kortbeek, J. Organomet. Chem. 33 (1971) v33;
(b) A. Horsfied, A. Wassermann, J. Chem. Soc. A (1970) 3202.
[29] J.F. Lee, M.D. Lee, P.K. Tseng, Chemistry 45 (1987) 50 (in Chinese).